CHAPTER 5

RESULTS AND DISCUSSIONS OF $0.02Ba(Mg_{1/3}Nb_{2/3})O_3$-$0.98BaTiO_3$ WITH LOW MELTING POINT ADDITIVES

From **CHAPTER 4** result, $0.02Ba(Mg_{1/3}Nb_{2/3})O_3$-$0.98BaTiO_3$ (BMN-BT) from P1 processing is of interest because of its high dielectric constant of about 40,000. However, the high sintering temperature of up to 1300 °C was employed. In order to reduce the sintering temperature has been carried on using liquid-phase sintering technique. The different sintering aids Bi_2O_3, Li_2CO_3 and PbO were used to prepare the ceramics with $0.02Ba(Mg_{1/3}Nb_{2/3})O_3$-$0.98BaTiO_3$ from P1 processing by conventional mixed-oxide method. Ceramics corresponding to the formula,

1. $(100\text{-}x)\ 0.02Ba(Mg_{1/3}Nb_{2/3})O_3\text{-}0.98BaTiO_3\text{-}xBi_2O_3/Li_2CO_3$

   where $2 \leq x \leq 10$,called S1 Ceramics

2. $(100\text{-}x\text{-}y)\ 0.02Ba(Mg_{1/3}Nb_{2/3})O_3\text{-}0.98BaTiO_3\text{-}xBi_2O_3/Li_2CO_3\text{-}yPbO$

   with $x : y$ = 1.32:0.43, 2.63:0.87 and 5.26:1.75, called S2 Ceramics

This chapter presents the results of the investigation on the role of sintering aids in $0.02Ba(Mg_{1/3}Nb_{2/3})O_3$-$0.98BaTiO_3$ ceramics. The contribution of a ceramic's extrinsic phenomena to its dielectric properties is discussed. The extrinsic phenomena which are related to the microstructural characteristics, grain characteristics, phase composition and crystallite characteristics.

PART I: The purpose of this part was to investigate the sintering behavior and the dielectric properties of (100-x) $0.02Ba(Mg_{1/3}Nb_{2/3})O_3$-$0.98BaTiO_3$ -xBi_2O_3/Li_2CO_3 system (S1 Ceramics) in view of attaining a transition temperature near room temperature.

5.1 Densification Measurement

In this part (I), the liquid phase sintering technique had been used to decrease the sintering temperature down to about 1000 °C. The chosen the sintering aids were Bi_2O_3 and Li_2CO_3 whose melting temperatures are 825 °C and 618 °C, respectively as the liquid phase formers in the sintering of $0.02Ba(Mg_{1/3}Nb_{2/3})O_3$-$0.98BaTiO_3$ ceramics. The without sintering aids sample (PART I) reached a full sintering temperature at 1300 °C and showed the maximum shrinkage value of about 16 %. Figure 5.1 (a) shows the effect of the sintering temperature on the linear shrinkages of the samples containing various sintering aids concentrations. It can be seen that the A sample (lowest concentration of x) reached a full shrinkage of 12 % at 1100 °C, whereas the other samples reached full shrinkage at low temperature at 850 °C. This result indicated that the shrinkage reach saturation at the low temperature as 850 °C with $x \geq 3$, i.e., the additives used can significantly reduce the sintering temperature of the ceramic down to around 1000 °C. Moreover, at $x = 3$ showed the maximum shrinkage value of about 19 %. For G sample (highest of $x = 10$), the final shrinkage decrease due to the Bi_2O_3/Li_2CO_3 (where Bi_2O_3/Li_2CO_3 indicated the equivalent mole of additives) formed a liquid phase at low temperature, which promoted sintering. However, over doped sintering aids did not form a liquid phase

or volatilize but rather remained in the samples and form a secondary phase, as confirmed by XRD results. Shrinkage in sintering aids additives samples indicated that sintering was complete at 900 °C, lower than the 1300 °C needed for the $0.02Ba(Mg_{1/3}Nb_{2/3})O_3$-$0.98BaTiO_3$. The dependence of shrinkage on Bi_2O_3/Li_2CO_3 addition also was confirmed by density in Figure 5.1(b); the final shrinkage temperature corresponded to the linear density. From the graph, it can be seen that at $x = 2$, showed the lowest density value of about 5.2 g/cm^3 due to the concentration of sintering aids is too small to promote the densification at low temperature (below 1000 °C), whereas the other composition ($x \geq 3$) reached full density at low temperature at 900 °C. After that the density values do not significant changes when increasing the sintering temperature. The maximum density was about 5.9 g/cm^3 with $x = 4$ sample. It should be noted that the high sintering temperature was needed to promote densification with an increased in fraction of sintering aids with $x = 2$-6. On the other hand, the decrease in density at $x = 10$ with increasing the sintering temperature may be due to the over added sintering aids did not form a liquid phase or volatilize but rather remained in the samples and form the greater amounts of liquid produce. Moreover, the intergranular porosity was formed and loose packing at this composition as seen in SEM micrograph in Figure 5.5.

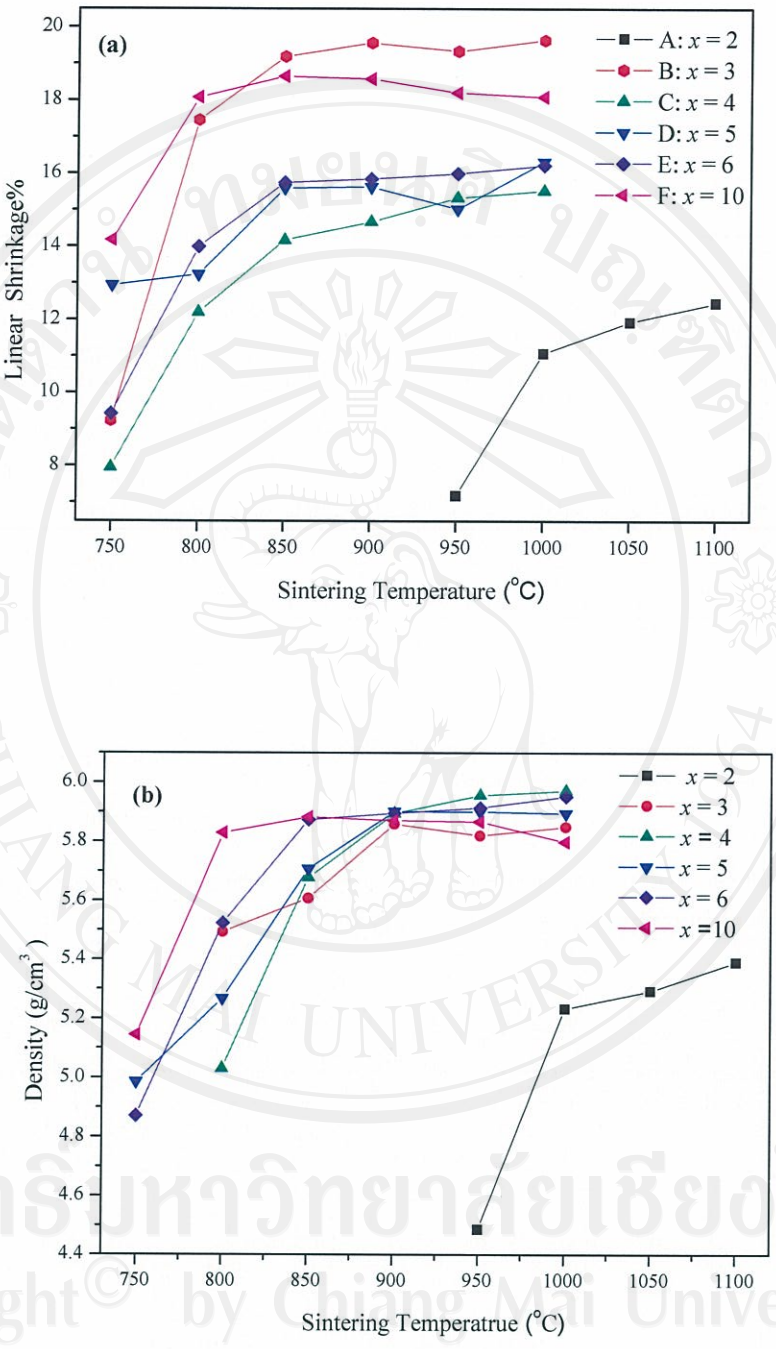

Figure 5.1 Linear shrinkage (a) and density (b) of (100-x) $0.02Ba(Mg_{1/3}Nb_{2/3})O_3$-$0.98BaTiO_3$-$xBi_2O_3/Li_2CO_3$ fired samples with as function of x against sintering temperature.

5.2 Phase Formation

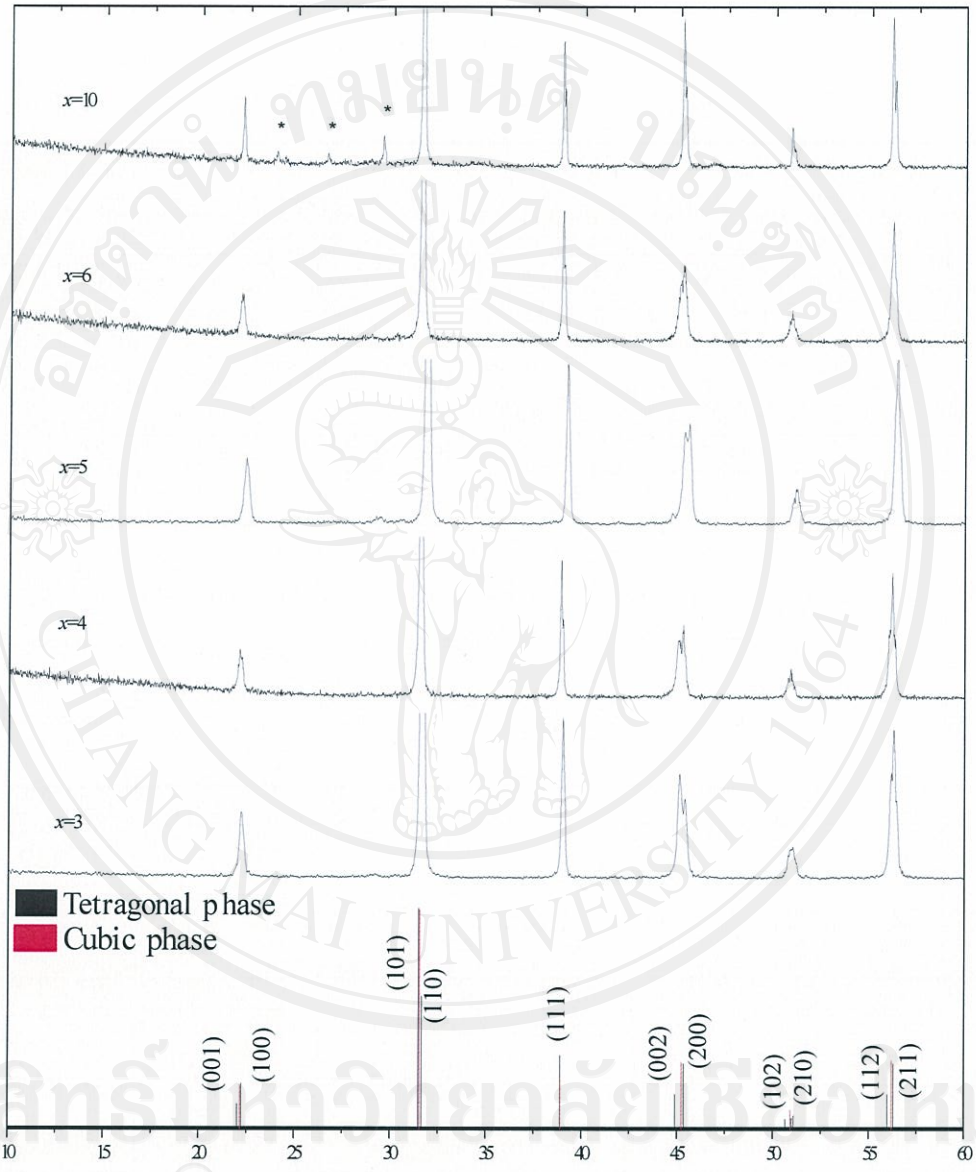

Figure 5.2 X-ray diffractions of (100-x) $0.02Ba(Mg_{1/3}Nb_{2/3})O_3$-$0.98BaTiO_3$ -xBi_2O_3/Li_2CO_3 samples with as function of x sintered at 950 °C and second phase formation; *indicating as second phases.

The influence of low sintering aids on phase formation and crystal structure of (100-x) $0.02Ba(Mg_{1/3}Nb_{2/3})O_3$-$0.98BaTiO_3$-$xBi_2O_3/Li_2CO_3$ ceramic was compared by XRD technique which detected at room temperature as a function of x. The XRD patterns of samples containing various sintering aids concentrations are shown in Figure 5.2. From the data, all of composition showed the shape peaks indicated the good crystalline which could be matched with BT as a main phase. Moreover, the splitting of peaks at high angle ($45° \leq 2\theta \leq 60°$) indicated the coexistence of cubic and tetragonal phases at room temperature were found with concentration of sintering aids between x = 3-6 whereas at x = 10, its crystal structure became pseudocubic as rhombohedral phase. It is widely accepted that the deformed cubic (psuedocubic) phase exists at room temperature. The lattice distortion that can occurs within BT added at room temperature is believed to be due to a replacement of Bi^{3+} and Li^{+} cations which have the different ionic radius. As can be seen, these changes were accompanied by a decrease in the *c/a* lattice parameter, and corresponding increased lattice strain with accompanying development of the pseudocubic phase.

The solid solubility of sintering aids Bi_2O_3/Li_2CO_3 in $0.02Ba(Mg_{1/3}Nb_{2/3})O_3$-$0.98BaTiO_3$ is expected to be limited. The XRD results obtained in this work confirm the expectation. The XRD profiles exhibited the second phase at x = 3 as been seen in Figure 5.2. The intensity of the diffraction peaks near 29.45°, 26.55° and 23.95° which corresponds to the secondary phase, also increased with increasing x. However, the shift of the diffraction peak due to increase the sintering temperature was not clearly to understand. Because of the sintered bodies exhibited a color change from red-brown to light yellow due to increasing the

sintering temperature, indicated that Bi^{3+} ion can diffuse in the matrix grains more than that at low temperature. According to literature [73-80], it is believed that Bi^{3+} and mostly Li^{+} cation undergo Ba-sites substitution. Therefore, the secondary phase was considered that Ba-sites in BT-based matrix grains were partially substituted by a small amount of Bi^{3+} and Li^{+} ion from sintering aids, while some Ba diffused out to grain boundary to form the stable compound of the Ba-Bi-Li-O system or a liquid phase along grain boundaries during sintering. A summarizes phases which were detected after the interactions as shown in TABLE 5.1. From the data, LBB: $LiBa_4Bi_3O_{11}$ [83] and BBT: $Ba_2Bi_4Ti_5O_{18}$ [81] were found as major second phase in all compositions to be a glassy phase and $Bi_{20}TiO_{32}$ was also detectable as a minor phase. A slightly different from the reported of Zhou [73] and his colleague who found the secondary phase as $Bi_2Ti_2O_7$ in BT-Bi_2O_3 ceramic system. It should be noted that can not detected the Bi_2O_3/Li_2CO_3 as an excess sintering aids at $x \leq 5$, indicated that the amount of Bi_2O_3/Li_2CO_3 was sufficient to produce the liquid phase sintering without residual but were deteriorated the percentage of perovskite in specimens. Moreover, $Ba_2Bi_4Ti_5O_{18}$ (JCPDS File No. 850923) [81] was found with increasing x and sintering temperature due to promote rise diffusion of Bi^{3+} ion into matrix grain. This result is quite agreed with Kuromitsu [79] who found $BaBi_4Ti_4O_{15}$ as secondary phase in BT-glass system.

The expectation of percentage of perovskite is to be decreased with increasing x and sintering temperature. The result obtained in this work confirms the expectation. The percentage of perovskite was plotted against fraction of x as shown in Figure 5.3. From the result, it can be seen that at $x = 10$, exhibited large amount of secondary phase were formed. But other composition showed the perovskite

saturation at the low temperature between 850°C - 950°C which exhibited the perovskite value was about over 96%. It should be noted that the increase in secondary phase was found to decrease the dielectric property such as ε_r.

Moreover, influence of sintering temperature on the ferroelectric phase as tetragonal has been found that at $x = 3$, the X-ray profiles of tetragonal splitting was increased with increasing the sintering temperature which exhibited the highest tetragonality (c/a) value of about 1.0067 in this study (in TABLE 5.1). This indicating more high temperature was required to promote ferroelectric phase in this composition. On the other hand, at $x = 4$ -10, the tetragonal phase was decreased with increasing sintering temperature due to decrease splitting of (200) and (002) peaks at high sintering temperature. Ferroelectric diminution phenomenon may be cause by high temperature promoted rise diffusion rate of sintering aids into BT lattice which effected on lattice defect or distortion.

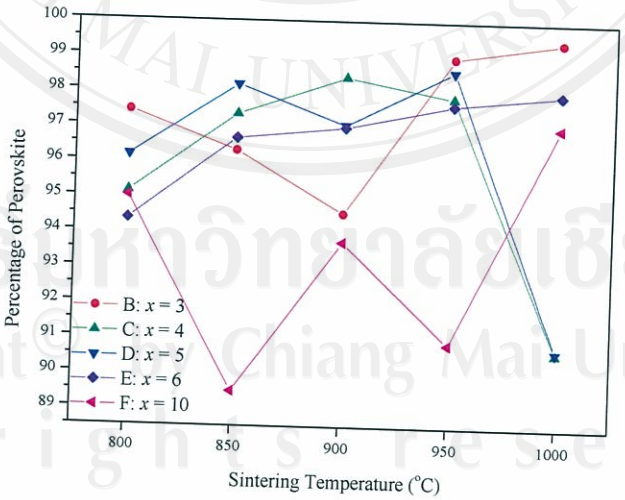

Figure 5.3 Percentage of perovskite of (100-x) 0.02Ba($Mg_{1/3}Nb_{2/3}$)O_3-0.98$BaTiO_3$ -xBi_2O_3/Li_2CO_3 samples with as function of x against sintering temperature.

TABLE 5.1 Phases identified by XRD in (100-x) $0.02Ba(Mg_{1/3}Nb_{2/3})O_3$-$0.98BaTiO_3$ -xBi_2O_3/Li_2CO_3 samples.

Composition,x(g)		% of Perovskite	c/a	Second phases
3	800 °C	97.4	No splitting	BBT, LBB
	850 °C	96.3	1.006	BBT, LBB
	900 °C	94.5	1.006	BBT, LBB
	950 °C	99	1.007	LBB
	1000 °C	99.4	1.006	LBB
4	800 °C	95.1	No splitting	BBT
	850 °C	97.3	1.005	BBT
	900 °C	98.4	1.004	BBT
	950 °C	97.8	1.005	BBT
	1000 °C	90.7	1.002	BiT, BBT
5	800 °C	96.2	No splitting	BBT, LBB
	850 °C	98.2	1.003	BBT, LBB
	900 °C	97	1.004	BBT, LBB
	950 °C	98.6	No splitting	LBB
	1000 °C	90.7	No splitting	LBB
6	800 °C	94.3	No splitting	L, B, BBT, LBB
	850 °C	96	1.0002	B, BBT
	900 °C	97	1.005	BBT
	950 °C	97.6	No splitting	BBT
	1000 °C	98	No splitting	BBT
10	800 °C	95	No splitting	B, L, LBB, BBT
	850 °C	89.5	No splitting	B, LBB, BBT
	900 °C	93.7	1.003	B, LBB, BBT
	950 °C	90.9	No splitting	LBB, BBT
	1000 °C	97	No splitting	BBT

n.b. B: Bi_2O_3, L: Li_2CO_3, BiT: $Bi_{20}TiO_{32}$ [82], LBB: $LiBa_4Bi_3O_{11}$ [83] and BBT: $Ba_2Bi_4Ti_5O_{18}$ [81]

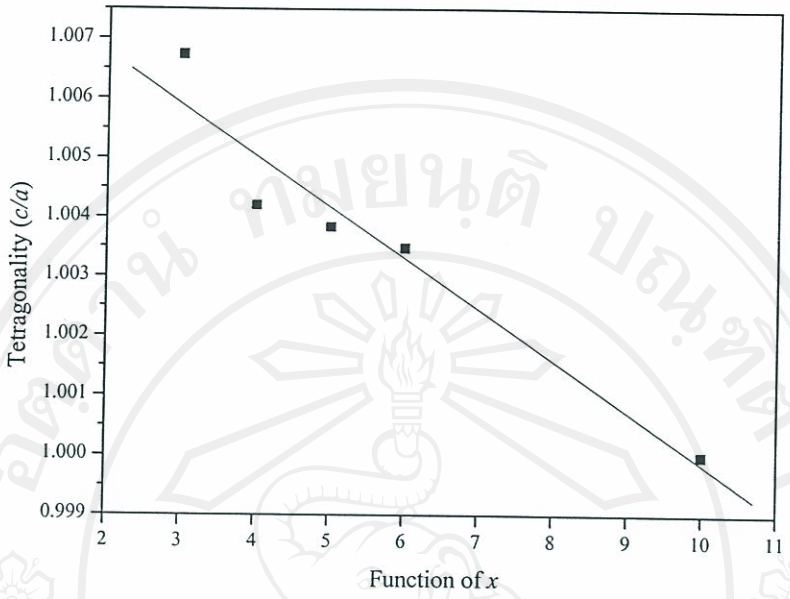

Figure 5.4 Tetragonality (*c/a*) of (100-*x*) $0.02Ba(Mg_{1/3}Nb_{2/3})O_3$-$0.98BaTiO_3$ -*x*Bi_2O_3/Li_2CO_3 samples with as function of *x* sintered at 950 °C.

5.3 Lattice Parameters Estimation

In general, the substitution of ions with different ionic sizes would distort the tetragonality of the lattice structure. A change in composition generally produces a change in lattice parameter and therefore, a shift in the position of the diffraction peaks of that phase (as seen in Figure 5.2). In this study, the *c/a* lattice parameter was calculate from splitting of (200) and (002) peaks at the angle 45° as shown in Figure 5.4. From the data, this has been shown the sintering aids cations can readily diffused into and be accommodated within the perovskite lattice. It has been found the increased Bi_2O_3/Li_2CO_3 concentration was also found to decrease the mean *c/a* lattice parameter of the BT-based ceramics, making it less tetragonal. This result is quite agreed with [77-80] who found this effect of Bi_2O_3/Li_2CO_3 on their system.

At x = 3-6, the *c/a* value remained almost constant. This suggests that the limit of solid solubility is x = 3, in agreement with the appearance of the $Ba_2Bi_4Ti_5O_{18}$. The decrease of the *c/a* lattice parameter can be attributed to the smaller ionic radius of Bi^{3+} (R_{Bi}~0.96 Å) and Li^{+} (R_{Li}~0.60 Å) compared to that of Ba^{2+} (R_{Ba}~1.6 Å). Also, these cations were found to have little solubility in BT. This result is quite agreed with Zhou [73] who found solubility limit of Bi_2O_3 in BT was about 3wt%. And 0.5wt% for Li_2CO_3 reported by Cheng and Li [69-72].

Moreover, the effect of sintering temperature on the *c/a* lattice parameter has been reported in TABLE 5.1. From the data, it was found that at x = 3, *c/a* ratio was slightly increased with increasing the sintering temperature meanwhile no significantly changes at x = 4. Whereas at x = 5, *c/a* value became to 1 due to decrease the (200) and (002) peaks splitting off with increasing the sintering temperature. This result indicated that at x = 3, more high temperature is needed to promote ferroelectric phase which exhibited the highest *c/a* value of about 1.007 with sintered at 950°C. And tetragonal phase diminution may be cause by high temperature promoted rise diffusion of sintering aids cations into BT lattice lead to lattice distortion. However, we expect that at x = 3, should be shown the good dielectric properties because its showed the low secondary phase, high density and good *c/a* lattice parameter value.

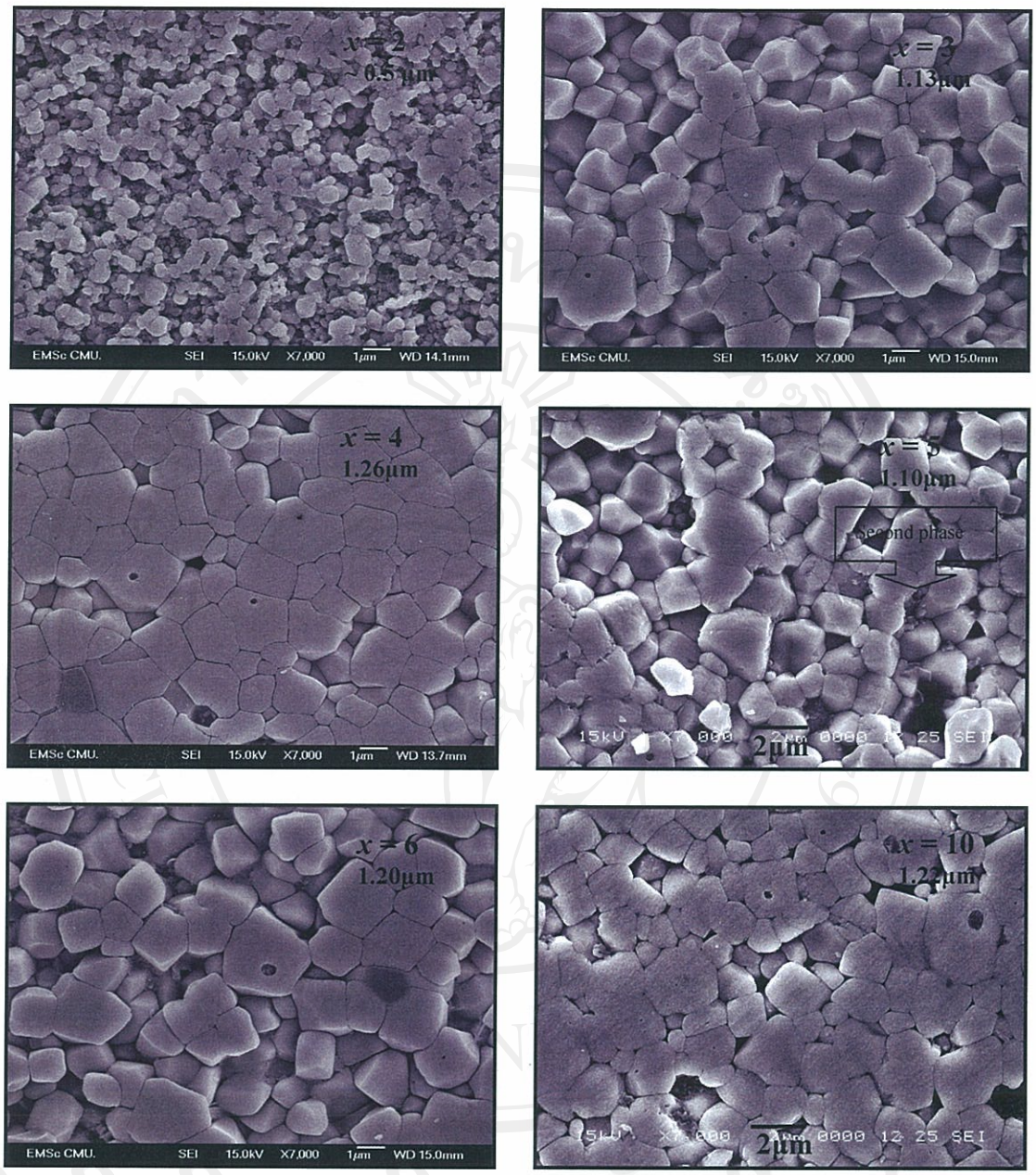

Figure 5.5 SEM micrograph of (100-x) $0.02Ba(Mg_{1/3}Nb_{2/3})O_3$-$0.98BaTiO_3$ -xBi_2O_3/Li_2CO_3 samples with as function of x with sintered at 950 °C.

5.4 Microstructure Evolution

The effect of low sintering aids, Bi_2O_3/Li_2CO_3 on the sintered $0.02Ba(Mg_{1/3}Nb_{2/3})O_3$-$0.98BaTiO_3$ ceramics is correlated with their densification and grain growth behavior. According to the literature [69-75] has been reported that grain growth was inhibited by liquid phase as inhibitor pinning at grain boundary. Moreover, Ba/Ti ratio has also influence on the microstructure evolution of BT-based ceramics as well. Many researchers [73-80] proposed that Bi^{3+} and Li^{+} cation undergo Ba-sites substitution. Meanwhile some Ba diffused out to grain boundary due to Bi^{3+} and Li^{+} substitution. Therefore, the A/B > 1, Ba excess promoted fine grain which is related to the suppression of grain growth due to formation of Ba-Bi-Li-O as secondary phase. In this study, we proposed that $LiBa_4Bi_3O_{11}$ was found by XRD technique. So, it can be speculated that Bi_2O_3/Li_2CO_3 addition suppressed the grain growth in $0.02Ba(Mg_{1/3}Nb_{2/3})O_3$-$0.98BaTiO_3$ ceramics.

The microstructure images against composition x has been shown in Figure 5.5. The result obtained in this work confirms the expectation. From the picture, it was found that at $x = 2$, the amount of sintering aids was not sufficient to reduce the sintering temperature down below 1000°C and the micrograph showed very poor densification. However, at $x \geq 3$, the grain growth was significantly inhibit, average grain size was decreased with respect to $0.02Ba(Mg_{1/3}Nb_{2/3})O_3$-$0.98BaTiO_3$. No abnormal grain growth is observed. The uniform fine grain was found at all composition and the grain size was about 1.10-1.26 μm. This result indicated that at $x = 3$ was sufficient to exhibit grain growth and to promote the densification. It should be noted that the grain size was not significantly changes with increasing x at the same sintering temperature. Moreover, at $x = 10$, showed the lowest density of

ceramic due to exhibit discontinuous grain size along with intergranular porosity in the specimen. This phenomenon reflected to decrease in the densification. The secondary phase started to detect at $x = 5$. Meanwhile at $x = 3$ - 4, showed the good packing and no evidence of the liquid phase coats grains and provides interconnection among them, indicating that the sintering aids, Bi_2O_3/Li_2CO_3 can diffuse into the matrix. This expectation can be investigated by EDX point analysis as can be shown in Figure 5.6.

For $x = 10$ specimen was used to be demonstration of element distribution because to avoid the resolution limited of instrument. Unfortunately, Li cation is a light element in periodic table which can not detected by this technique. Therefore, in this study, we concerned about distribution of Bi element only. From the Backscatter images, it can be seen the coexistence of two phases in bulk ceramic as uniform matrix phase and bismuth rich phase at intergranular layers (white areas). Concerning at intergranular region between the grain boundaries, the EDX data showed the Bi precipitate along grain boundary indicated that bismuth rich phase was found as secondary phase. Moreover, Ba atom was found coexistence in this phase. This result can confirm that Ba element can diffuse out of matrix due to substitute by sintering aids and form the second phase at grain boundary. The Ba: Bi: O ratio is given approximately 7.7:18.08:35. Therefore, this phase suggests to be $Ba_2Bi_3O_9$ but the XRD data showed the $LiBa_4Bi_3O_{11}$ as second phase. The slightly different result is due to error from can not detect Li ion. This may be cause by total weight not equal 100%. In case matrix (Figure 5.6 (B), (C)), it was found that Bi content was decreased with increasing the distance from grain boundary to center of grain.

From this result, it can suggest that chemical concentration gradient of Bi cation was occurred in this system.

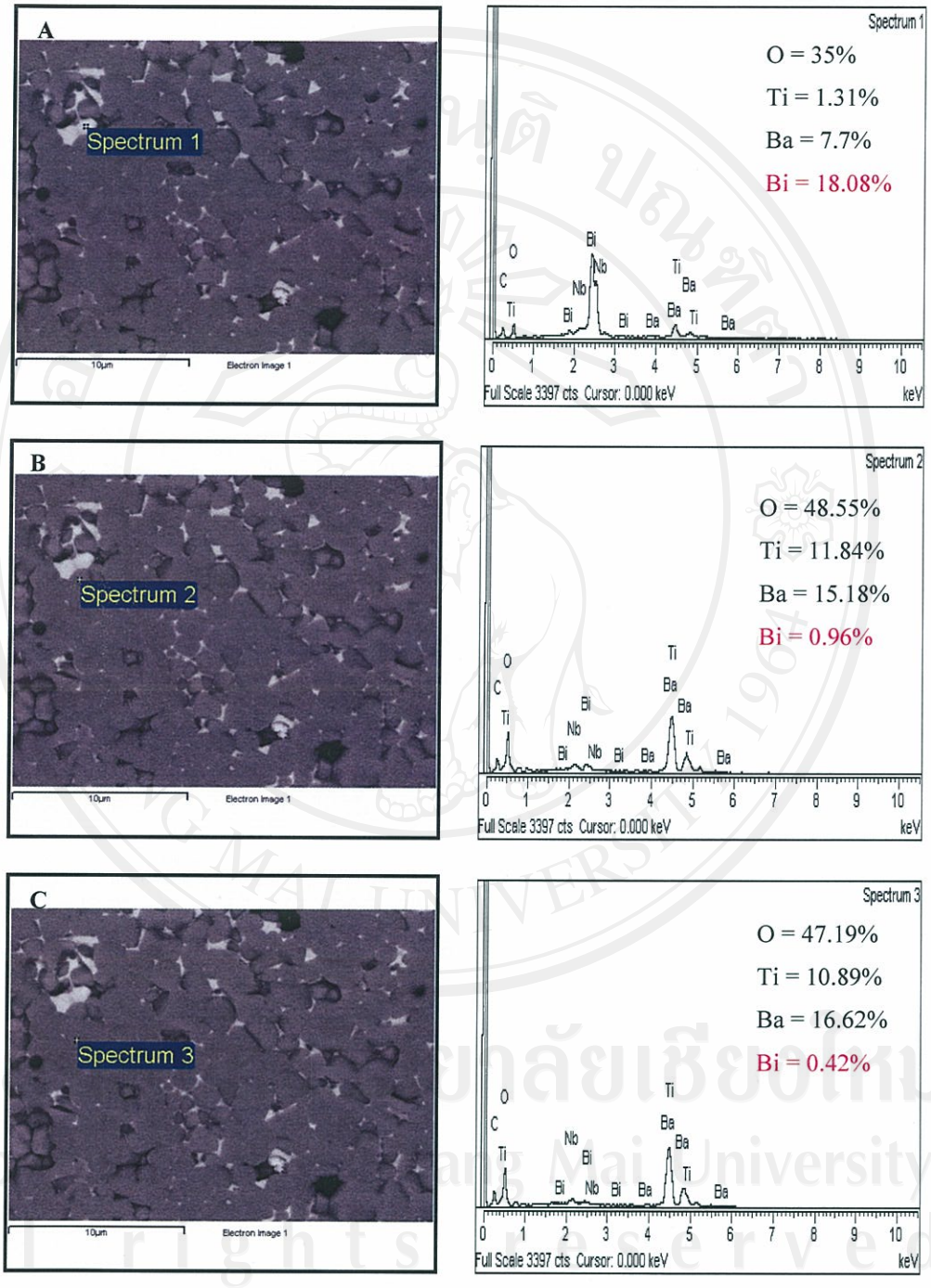

Figure 5.6 Backscattered images of $x = 10$ specimen sintered at 950°C; (A) EDX from intergranular region labeled "spectrum1"; (B) and (C) EDX from matrix grain labeled "spectrum2 and 3".

5.5 Dielectric Properties

In general, addition of the sintering aids to BT-based was found to beneficially reduce the sintering temperatures but lower ε_r was obtained. The result obtained in this work confirms the expectation. The ε_r -T peak was plotted against composition x as shown in Figure 5.7. The observed dielectric characteristics can be seen that ε_r decreases compared with that of un-sintering aids $0.02Ba(Mg_{1/3}Nb_{2/3})O_3$-$0.98BaTiO_3$, suggesting Ba-sites substitution of Li^+ and Bi^{3+}. The lowing of the T_c also confirms this point of view [70]. From the graphs, it can be seen that the peak of the diffuse tetragonal-cubic transition occurred at a temperature much lower than the regular transition temperature (result from Part I, T_c ~ 88°C, ε_r = 40,000), and the ε_r-value decreased remarkably to 3,000.

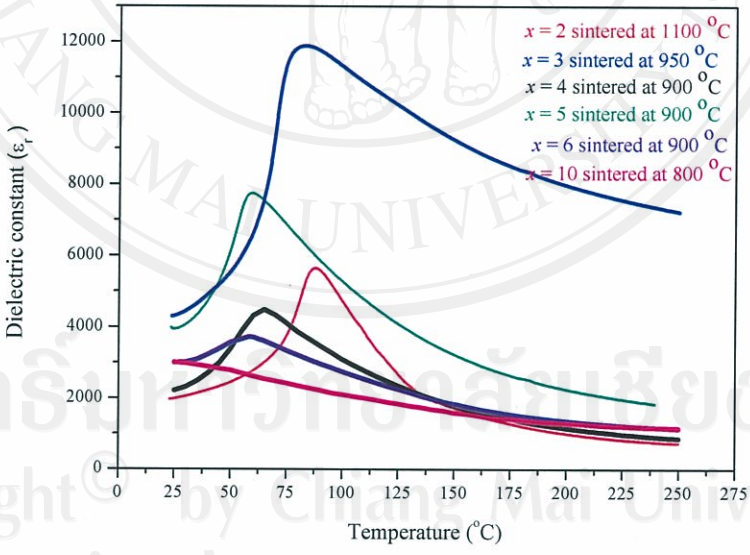

Figure 5.7 Temperature variation of dielectric constant ε_r of the (100-x) $0.02Ba(Mg_{1/3}Nb_{2/3})O_3$-$0.98BaTiO_3$-$xBi_2O_3/Li_2CO_3$ with as function of x at 1 kHz.

It has been found the greater Bi_2O_3/Li_2CO_3 concentration, the smaller is the ε_r-value obtained of about 3,000. In this case, the ε_r-T peak was completely suppressed and flat temperature dependence of dielectric response resulted, as indicated by the ε_r-T curve of at x = 10 specimen as shown in Figure 5.7. The flattening of the transition region was attributed to the formation of a pseudocubic phase as rhombohedral phase, in agreement with result of Armstrong [21] and Lin [84] for BT system. It is notable that the ε_r-T characteristics of specimens are intimately related to their microstructure. The specimens which possess diffuse ε_r-T peak response all maintain the ultra-fine grain structure. The maximum dielectric constants ε_{max} and T_c as a function of the concentration x are presented in Figure 5.8. The data showed the dielectric behavior of this system depend on the concentration of sintering aids ratio and tend to decrease when increasing amount of sintering aids content.

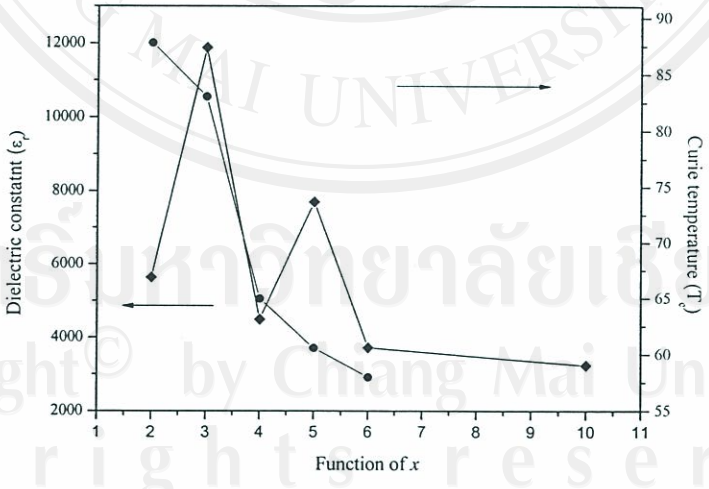

Figure 5.8 Maximum dielectric constant and transition temperature of $(100\text{-}x)0.02Ba(Mg_{1/3}Nb_{2/3})O_3\text{-}0.98BaTiO_3\text{-}xBi_2O_3/Li_2CO_3$ samples versus function of x.

Moreover, T_c was found to shift downward, indicated that Bi^{3+} and Li^{+} cation can diffuse into Ba-sites. This result was confirmed by EDX technique as shown in Figure 5.6. From the data, the maximum ε_r increased from 5,600 to 12,000 in the composition range $2 \leq x \leq 3$, then decreased within the composition $x = 4$. After that, at $x = 5$, specimen showed the ε_r increased to 7,700 and dropped this value again when increasing $x > 5$. The T_c decreased continuously with increasing in x. It should be noted that at between range $3 \leq x \leq 4$, T_c was remarkably decreased from 83°C to 65°C. It can suggest that at $x = 3$ was a critical concentration because of its dielectric properties was significantly change at this concentration.

According to dielectric loss, Figure 5.9 showed the temperature dependence of the tanδ at 1 kHz.

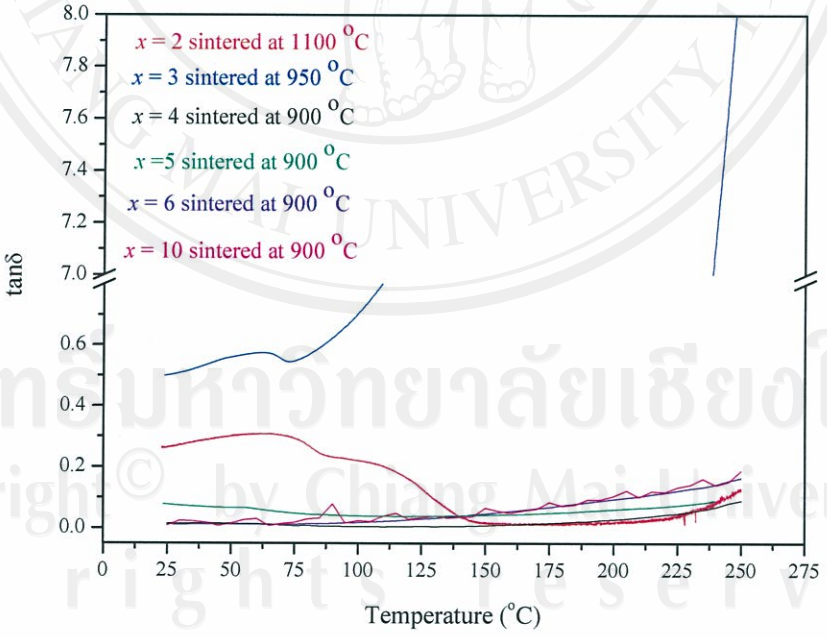

Figure 5.9 Temperature variation of dielectric loss tanδ of the (100-*x*) $0.02Ba(Mg_{1/3}Nb_{2/3})O_3$-$0.98BaTiO_3$-$xBi_2O_3/Li_2CO_3$ with as function of x at 1 kHz.

It was observed that, for the Bi_2O_3/Li_2CO_3 addition specimens, tanδ slightly increased at room temperature and tended to increase with increasing the temperature, compared with un-sintering aids. Especially at $x = 3$ specimen presented the maximum value of tanδ was about 0.615 and tended to warped upwards markedly when temperature is higher that 75°C of about 8, compared with un-sintering aids specimen (tanδ ~ 0.085). It may be due to substituted Li^+ and Bi^{3+} at Ba-sites can be taken as an accepter and donor in BT lattice. So, in this study, Bi_2O_3 and Li_2CO_3 are added in equivalent mole. Therefore, in order to balance out the charge fluctuation and to suppress the possibility of defect formation cause by different cation. In charge balance compensation mechanism are following defect reaction equations.

For Bi^{3+} ions,

$$Bi_2O_3 + 2Ba_{Ba} \rightarrow 2Bi^{\bullet}_{Ba} + V''_{Ba} + 2BaO \qquad (2.10)$$

For Li^+ ions,

$$Li_2O + 2Ba_{Ba} + O_O \rightarrow 2Li'_{Ba} + V_O^{\bullet\bullet} + 2BaO \qquad (2.11)$$

It can be seen that the defect is still occurred in material by nature. So, considering the possible defects were occurred in the system as $Bi^{\bullet}_{Ba}, V''_{Ba}$, Li'_{Ba} and $V_O^{\bullet\bullet}$. It may be cause by the influence of leakage conductivity. On the other hand, the rapid increase of tanδ at high temperature may be due to the interstitial effect with Li^+ (because owing to its small ionic radius, Li^+ is mobile in ceramics) can be confirmed by the anomalous increase of tanδ when temperature is higher than T_c. Furthermore, the constriction of volume when the phase changes from a tetragonal to cubic lattice structure will make the interstitial ions unstable and tanδ is increased abruptly. This result is agreed with Cheng [69-70] who found the Li^+ replaced the Ti-

site, the high value of tanδ was obtained. This effect may enforce the interstitial adding of Li^+ because of its rather smaller ionic radius compared with Ba^{2+}. Arising from the interstitial ions, increased temperature gives more vibrating energy to the lattice ions and increases in tanδ.

From the dielectric data, it was found that the T_c decreases accompanied by peak broadening, with increasing x. The broadness, δ_γ and diffusivity, γ are estimated by plots of Log $[(\varepsilon_{max}/\varepsilon)-1]$ versus Log (T-Tm) were generated for $0 \leq x \leq 10$, as shown in Figure 5.10. The mean value of δ_γ and γ are calculated from equation 4.1 as can be shown in TABLE 5.2. In (100-x) $0.02Ba(Mg_{1/3}Nb_{2/3})O_3$-$0.98BaTiO_3$-$xBi_2O_3/Li_2CO_3$ system, the value of γ varies between 1.3-1.54, which confirmed the diffuse phase transitions due to the compositional fluctuation and structural disordering in the arrangement of cations in one or more crystallographic sites of the structure. It was found that the γ value was decreased, which compared with un-sintering aids $0.02Ba(Mg_{1/3}Nb_{2/3})O_3$-$0.98BaTiO_3$ specimen (γ = 1.57). Moreover, the δ_γ values of compositions in this system were found in range 10.94-22.52. It suggests that the fine grain become more homogeneity due to enhanced solid diffusion of Bi_2O_3/Li_2CO_3 into grain.

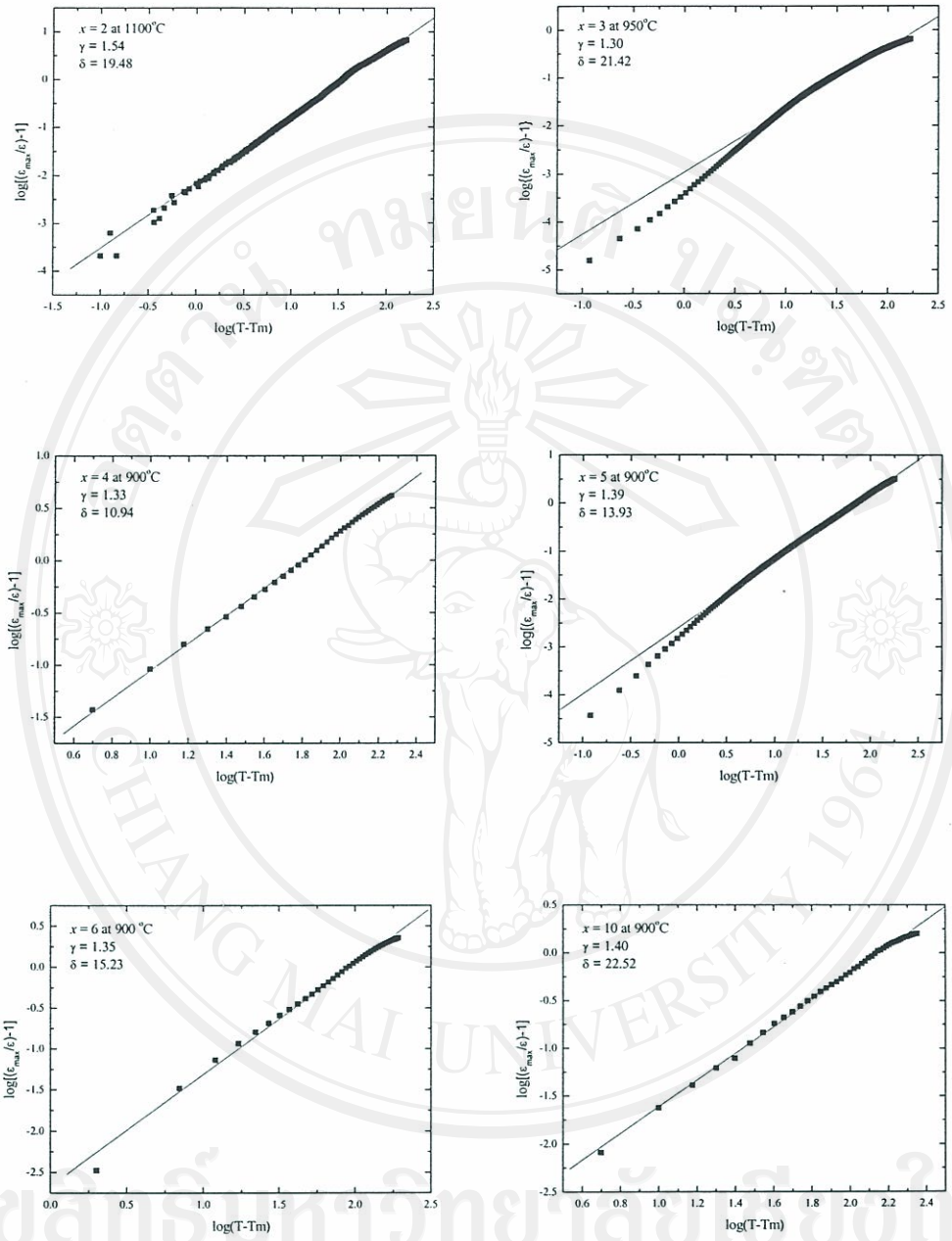

Figure 5.10 Log[($\varepsilon_{max}/\varepsilon$)-1] vs Log(T-Tm) for (100-x) 0.02Ba($Mg_{1/3}Nb_{2/3}$)O_3-0.98$BaTiO_3$ -xBi_2O_3/Li_2CO_3 ceramics, x = 2, 3, 4, 5, 6 and 10 with prepared by S1 processing.

TABLE 5.2 Dielectric properties of $(100\text{-}x)0.98BaTiO_3\text{-}0.02Ba(Mg_{1/3}Nb_{2/3})O_3\text{-}xBi_2O_3/Li_2CO_3$ where $2 \leq x \leq 10$ (S1 Ceramics).

Composition of x	T_{max} (°C)	ε_{max} at 1 kHz	tanδ at T_{max}	ε_r at 25°C	tanδ at 25°C	γ	δ_γ	ρ(Ω.cm)	Avg grain size (μm)
0(1300°C)	88	43,000	0.085	38,787	0.068	1.57	25.38	7.9×10^7	5.54
2(1100°C)	88	5,639	0.233	1,954	0.265	1.54	19.48	-	2.10
3(950°C)	83	11,880	0.615	4,346	0.571	1.29	21.42	3.9×10^6	1.13
4(900°C)	65	4,489	0.011	2,238	0.015	1.33	10.94	-	1.26
5(900°C)	60	7,738	0.061	3,964	0.077	1.39	13.93	1×10^{12}	1.10
6(900°C)	58	3,715	0.012	3,000	0.012	1.35	15.23	-	1.20
10(900°C)	-	2,994	0.009	2,994	0.09	1.40	22.52	1×10^7	1.22

PART II: The purpose of this part was to investigate the effect of PbO on the sintering behavior and the dielectric properties of (100-x-y) $0.02Ba(Mg_{1/3}Nb_{2/3})O_3$-$0.98BaTiO_3$-$xBi_2O_3/Li_2CO_3$-$yPbO$ system (S2 Ceramics) in view of attaining a transition temperature near room temperature. According to preparation of the specimen composition as shown in TABLE 5.3

TABLE 5.3 Sample compositions of (100-x-y) $0.02Ba(Mg_{1/3}Nb_{2/3})O_3$-$0.98BaTiO_3$-$xBi_2O_3/Li_2CO_3$-$yPbO$ ceramics.

Process	Code	Sample composition		
		$0.02Ba(Mg_{1/3}Nb_{2/3})O_3$-$0.98BaTiO_3$ From P1 processing (g)	Bi_2O_3/Li_2CO_3 x(g)	PbO y(g)
S2	BT-BMN	100	-	-
	A	98.25	1.32	0.43
	B	96.50	2.63	0.87
	C	92.99	5.26	1.75

n.b. Sample compositions are of the form

(100-x-y) $0.02Ba(Mg_{1/3}Nb_{2/3})O_3$-$0.98BaTiO_3$ -xBi_2O_3/Li_2CO_3-$yPbO$

5.6 Densification Measurement

In this part (II), the chosen the sintering aids were equivalent mole of Bi_2O_3/Li_2CO_3 and PbO whose melting temperatures are 825°C, 618°C and 880°C, respectively as the liquid phase formers in the sintering of $0.02Ba(Mg_{1/3}Nb_{2/3})O_3$-$0.98BaTiO_3$ ceramics. Figure 5.11 showed the effect of the sintering temperature on the linear shrinkages and densities of the specimens containing various sintering aids concentrations. (Figure 5.11(a)) The shrinkage of the specimens with sintering aids all showed significant increase starting from for temperature higher than 750°C and tends to be saturated after sintering at 850°C, sintering above 900°C results showed no significant change. Similar trend was also found with the $0.02Ba(Mg_{1/3}Nb_{2/3})O_3$-$0.98BaTiO_3$ specimens but at higher temperature. The maximum shrinkage value about 20% was achieved with highest amount of sintering aids (Sample C) at lower sintering temperature of about 750°C. From the result, the linear shrinkage was increased by increasing amount of sintering aids at lower sintering temperature. This reveals that the microflow of the liquid phase accelerates the sintering process.

For density value, at 900°C, the Sample A possessed a density higher than 94% of the theoretical density. In contrast, the C specimen with the sintering temperature about 800°C, its density slightly decreased at high sintering temperature, from about 90% of the theoretical density. This may be due to the vaporization of Bi_2O_3/Li_2CO_3 and PbO. However, all of amount of sintering aids is sufficient for low sintering as 1000°C in this system.

For both results, it can be seen that the density and shrinkage reach saturation at the temperature as low as 850°C, i. e., the sintering aids used can significantly reduce the sintering temperature of the ceramic down to around 900°C.

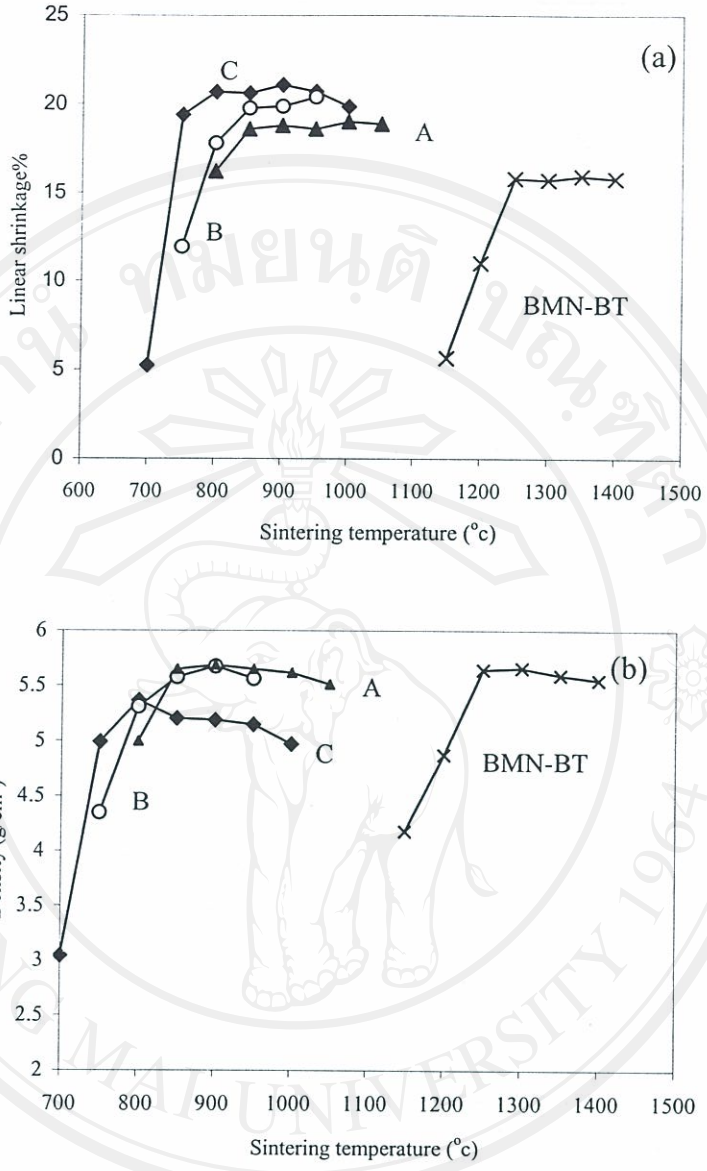

Figure 5.11 Linear shrinkage (a) and Density (b) of (100-*x*-*y*) $0.02Ba(Mg_{1/3}Nb_{2/3})O_3$-$0.98BaTiO_3$ -xBi_2O_3/Li_2CO_3-$yPbO$ fired samples containing different amounts of sintering aids against sintering temperature.

5.7 Phase Formation

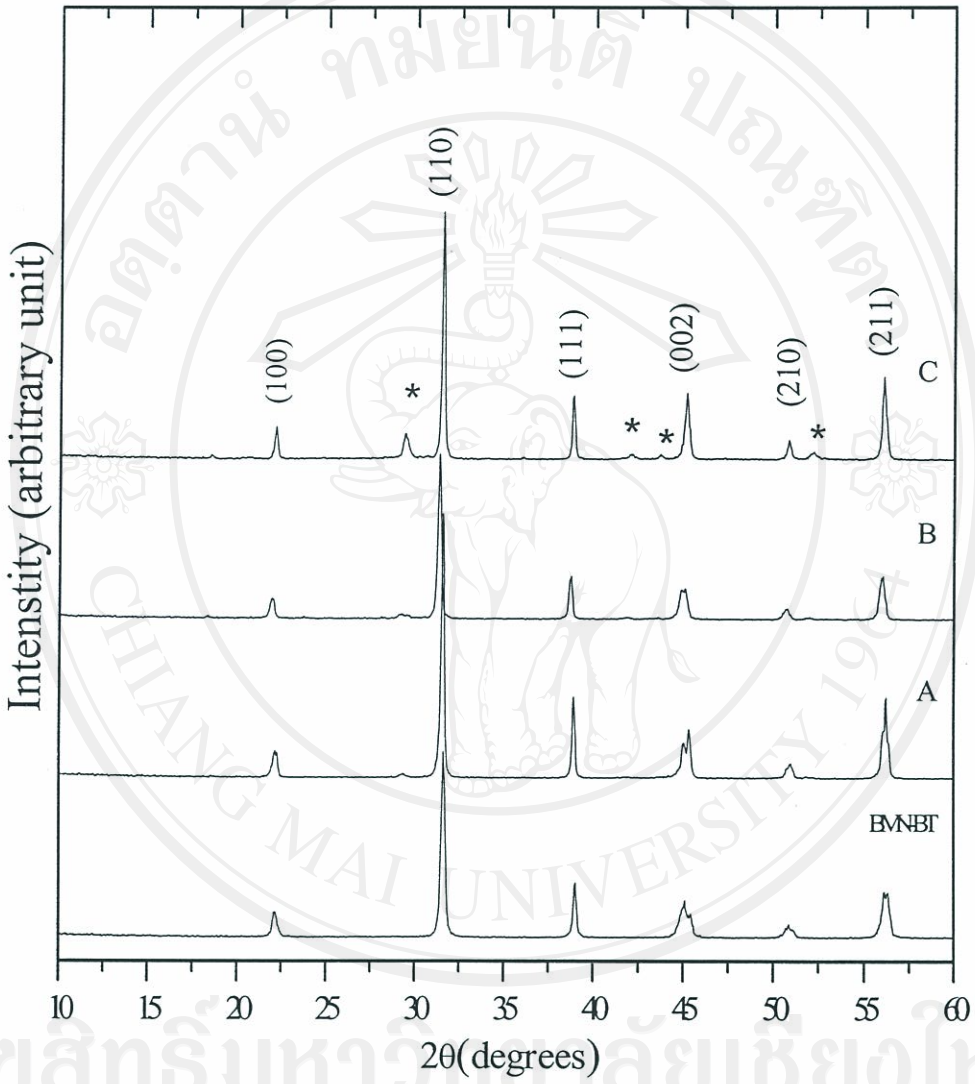

Figure 5.12 X-ray diffractions of (100-*x*-*y*) $0.02Ba(Mg_{1/3}Nb_{2/3})O_3$-$0.98BaTiO_3$ -*x*Bi_2O_3/Li_2CO_3-*y*PbO samples with as function of *x,y* sintered at 950 °C and second phase formation; *indicating as second phases.

The XRD patterns of specimens containing various sintering aids concentrations are shown in Figure 5.12. These patterns reveal that the samples containing small amounts of sintering aids (Sample A) has the tetragonal perovskite structure. This can be attributed to the diffusion of some amounts of sintering aids into the $0.02Ba(Mg_{1/3}Nb_{2/3})O_3$-$0.98BaTiO_3$ lattices and as a result the ceramic can not retain the coexistence of tetragonal and cubic phases at room temperature. It is also evident that the tetragonal-cubic transformation occurred in Sample B at room temperature while Sample C contained multiphases, with the cubic structure as a major phase and $LiBa_4Bi_3O_{11}$ as a second phase. Moreover, $BaBi_4Ti_5O_{18}$ and $BaLi_4$ [85] were found coexistent with $LiBa_4Bi_3O_{11}$ in all composition. However, $BaBi_4Ti_5O_{18}$ and $BaLi_4$ were decreased with increasing the sintering temperature due to promote of rise segregation of sintering aids at intergranular region (cause found only $LiBa_4Bi_3O_{11}$). Also, we did not observe Pb-compound in the XRD analysis, perhaps because of its small quantity or may be cause by high reactivity of Pb ion to promote the diffusion.

The expectation of percentage of perovskite is to be decreased with increasing *x,y* and sintering temperature. The result obtained in this work confirms the expectation. The percentage of perovskite was plotted against fraction of *x,y* as shown in Figure 5.13. From the result, it can be seen that Sample A exhibited the small amount of second phase and showed the high value of perovskite phase was about > 98%. It should be noted that the % perovskite was not significant change with increasing sintering temperature. This is may be due to the small amount of sintering aids (total 1.75 wt%) are diffused into matrix and disappeared to segregate at intergranular region. This result can confirm by SEM image in Figure 5.16 A.

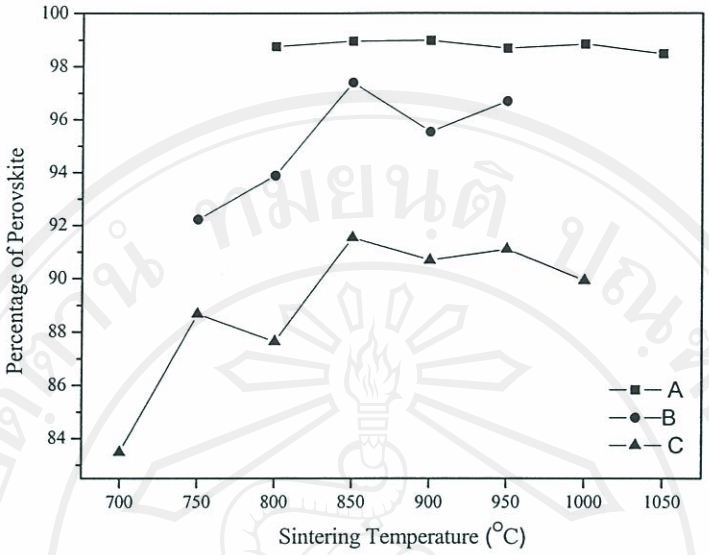

Figure 5.13 Percentage of perovskite of (100-x-y) 0.02Ba($Mg_{1/3}Nb_{2/3}$)O_3-0.98$BaTiO_3$ -$x$$Bi_2O_3$/$Li_2CO_3$-$y$PbO system with as function of x,y against sintering temperature.

Vice versa, Sample C showed the lowest value of perovskite due to the large of second phase was found. The maximum value of perovskite was about 92% which found at 850°C and tended to decrease with increasing sintering temperature due to the increasing the glass former segregated at intergranular as can see in Figure 5.16 C. However, it should be noted that the ε_r -T characteristics of specimens are intimately related to the second phase as impurity.

5.8 Lattice Parameters Estimation

In general, the substitution of different cations will depend on the radius of the ion and its chemical properties such as valency and electronegativity. According to the principles of crystal chemistry, it is expected that Bi^{3+}, Li^{+} and Pb^{2+}ions prefer to enter Ba-sites in perovskite structure. Figure 5.14 shows the lattice parameter of

Sample A at various sintering temperature. In the pseudocubic phase at low temperature, the lattice parameter decreased gradually with increasing sintering temperature, and in the tetragonal phase at above 900°C, the *c/a* ratio increased with increasing sintering temperature. In tetragonal phase, *c* increased slightly with increasing sintering temperature, whereas the value of *a* decreased but not significantly change with sintering temperature, which results in enhancement in the tetragonality of Sample A. This result indicated that Sample A is needed high temperature to promote ferroelectric phase which exhibited highest *c/a* ratio of about 1.0078 with sintered at 1000°C.

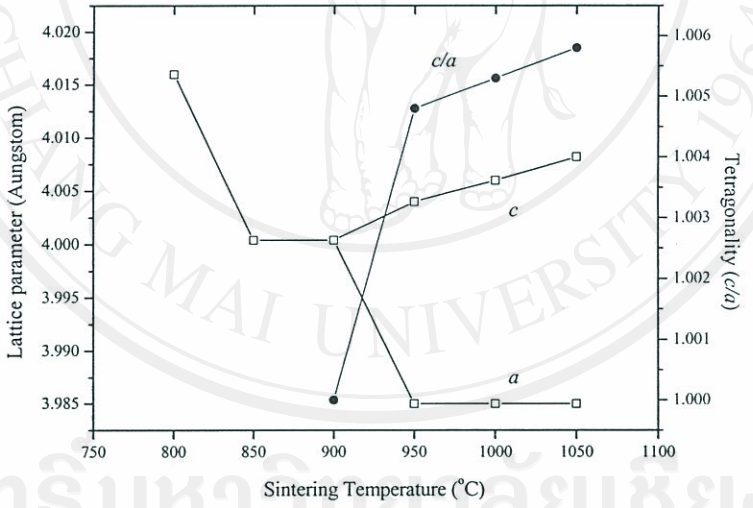

Figure 5.14 Lattice parameter *(c/a)* of $98.25[0.02Ba(Mg_{1/3}Nb_{2/3})O_3\text{-}0.98BaTiO_3]$ $\text{-}1.32Bi_2O_3/Li_2CO_3\text{-}0.43PbO$ samples (Sample A) against sintering temperature.

However, when the Bi_2O_3/ Li_2CO_3-PbO content increased, the tetragonal splitting peaks disappear, indicating that degree of the tetragonality (*c/a*) decreased.

This result can confirm by XRD data in Figure 5.12. The perovskite phase appears to have pseudocubic symmetry for Sample C and tetragonal symmetry for Sample A and B corresponding with increasing sintering temperature. This data indicated that at Sample C, the sintering aids can completely suppress the tetragonal phase formation. It can be seen in Figure 5.15, at Sample C, the value of *a* lattice parameter tended to decrease with increasing sintering temperature. The decrease of the lattice parameter, *a* can be attributed to the smaller ionic radius of Bi^{3+} (R_{Bi}~0.96 Å) and Li^{+} (R_{Li}~0.60 Å) compared to that of Ba^{2+} (R_{Ba}~1.6 Å). And tetragonal phase diminution may be cause by high temperature promoted rise diffusion of sintering aids cations into BT lattice lead to lattice distortion. The influence of sintering aids on the lattice parameter has been reported in TABLE 5.3.

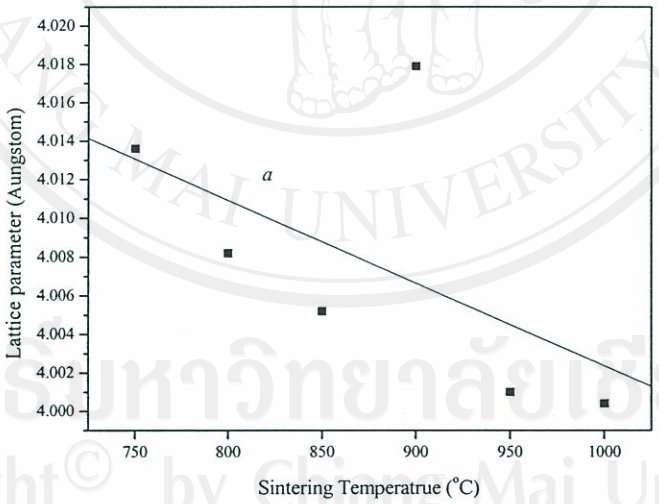

Figure 5.15 Lattice parameter (*a*) of 92.99[0.02Ba($Mg_{1/3}Nb_{2/3}$)O_3-0.98$BaTiO_3$] -5.26Bi_2O_3/Li_2CO_3-1.75PbO samples (Sample C) against sintering temperature.

TABLE 5.4 Phases identified by XRD in (100-*x*-*y*) $0.02Ba(Mg_{1/3}Nb_{2/3})O_3$-$0.98BaTiO_3$ -xBi_2O_3/Li_2CO_3-*y*PbOsystem.

Materials	Sintering Temperature (°C)	Density (g/cm^3)	Lattice Parameter			% of Perovskite
			a (Å)	*c* (Å)	*c/a*	
0.98BT0.02BMN	1300	5.81	3.9920	4.0152	1.0058	100
A	800	5	4.0160	-	No splitting	98.75
	850	5.65	4.0004	-	No splitting	98.95
	900	5.69	4.0004	-	No splitting	98.97
	950	5.65	3.9850	4.0040	1.0048	98.68
	1000	5.62	3.9850	4.0160	1.0078	98.84
	1050	5.51	3.9850	4.0082	1.0058	98.48
B	750	4.35	3.985	-	No splitting	92.22
	800	5.31	3.985	-	No splitting	93.88
	850	5.58	4.0004	-	No splitting	97.39
	900	5.67	3.985	-	No splitting	95.53
	950	5.56	4.0160	4.0238	1.0019	96.69
C	700	3.04	4.001	-	No splitting	83.48
	750	4.99	4.0136	-	No splitting	88.67
	800	5.37	4.0082	-	No splitting	87.64
	850	5.20	4.0052	-	No splitting	91.53
	900	5.19	4.0179	-	No splitting	90.68
	950	5.15	4.001	-	No splitting	91.10
	1000	5	4.0004	-	No splitting	98.92

5.9 Microstructure Evolution

According to chemical reasons, most Li^{+}, Bi^{3+} and Pb^{2+} ions replaced the Ba-sites substitution, which results in increasing in the amount of Ba diffused out to grain boundary in this system. In the case of Ba > 1, Ba excess is related to the suppression of grain growth due to the formation of second phase. The phase transition became diffuse was reported in this case. Expectation that the grain size was decreased with increasing the amount of sintering aids. The result of sintering aids effect on microstructure was shown in Figure 5.16.

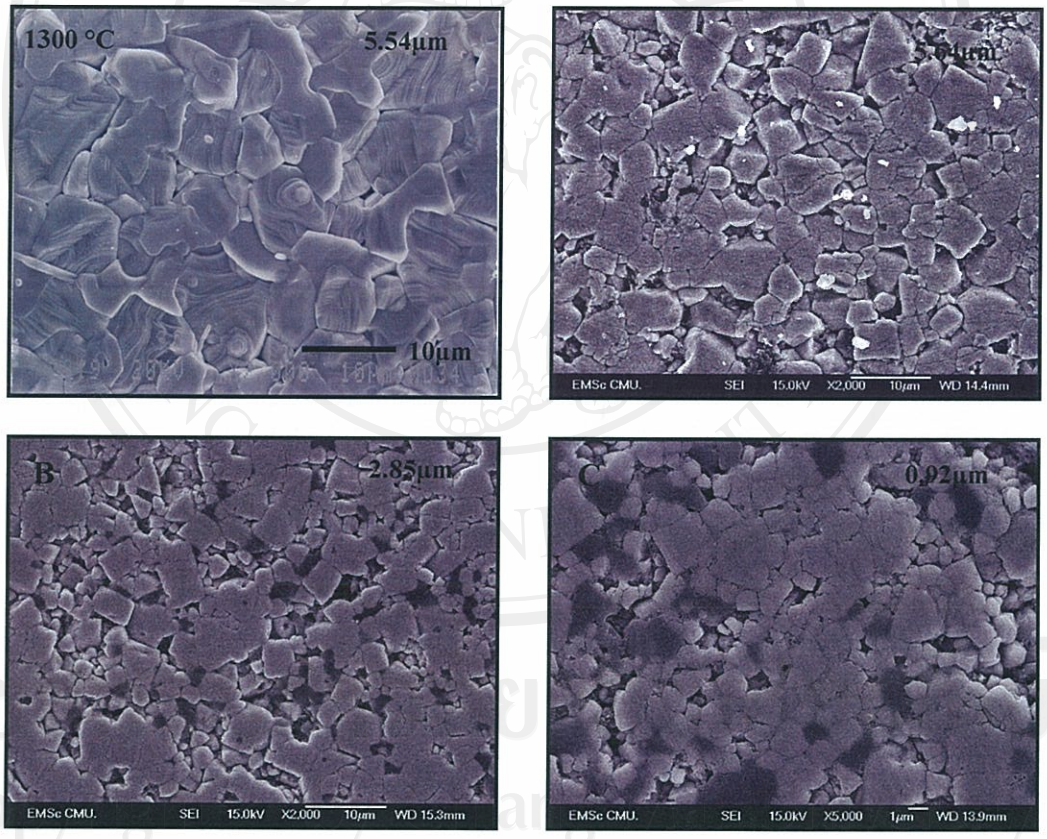

Figure 5.16 Microstructures of (100-x-y) 0.02Ba($Mg_{1/3}Nb_{2/3}$)O_3-0.98$BaTiO_3$ -$x$$Bi_2O_3$/$Li_2CO_3$-$y$PbO ceramics sintered at 950 °C for 2 h.

Figure 5.16 reveals the observation of chemically etched, polished ceramic surfaces of Sample A, B and C by scanning electron microscopy. The microstructure evolution and size distribution in each sample is reasonably homogeneous and the average grain sizes of Sample A, B and C are 5.64, 2.85 and 0.92 μm, respectively. The inhibition of grain growth was observed in all samples caused by secondary phases, $BaBi_4Ti_5O_{18}$, $LiBa_4Bi_3O_{11}$ and $BaLi_4$ were formed at intergranular region to be grain growth inhibitor. This same result was realized by Li and Cheng [69, 70, 72]. From the micrographs, it was found that the liquid phase coats grains and provides interconnection among them. Moreover, the polygonal grain shape became fine grain with round shape was found with increasing the concentration of sintering aids.

We expected that the black areas between grains are the site of high reactivity of secondary phase compound which reacted with etching acid during specimen preparation.

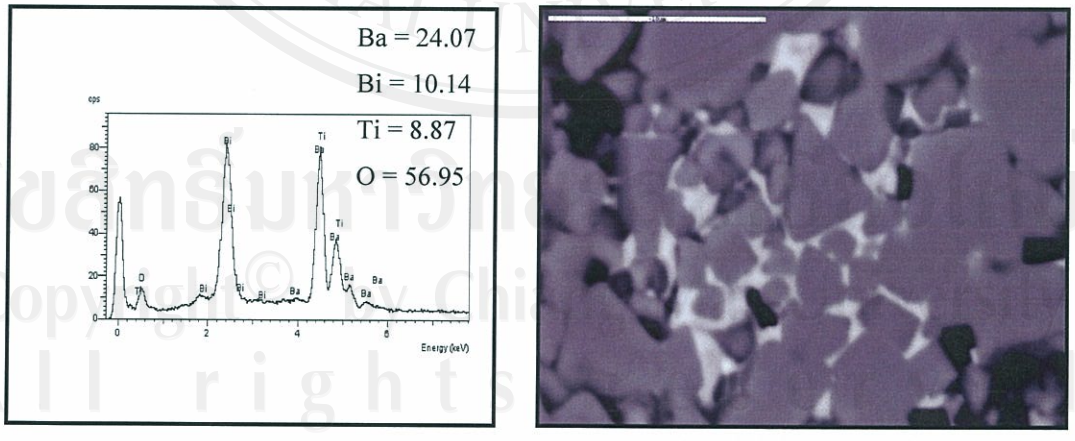

Figure 5.17 Backscattered images and EDX of Sample B sintered at 950°C at intergranular region (white area).

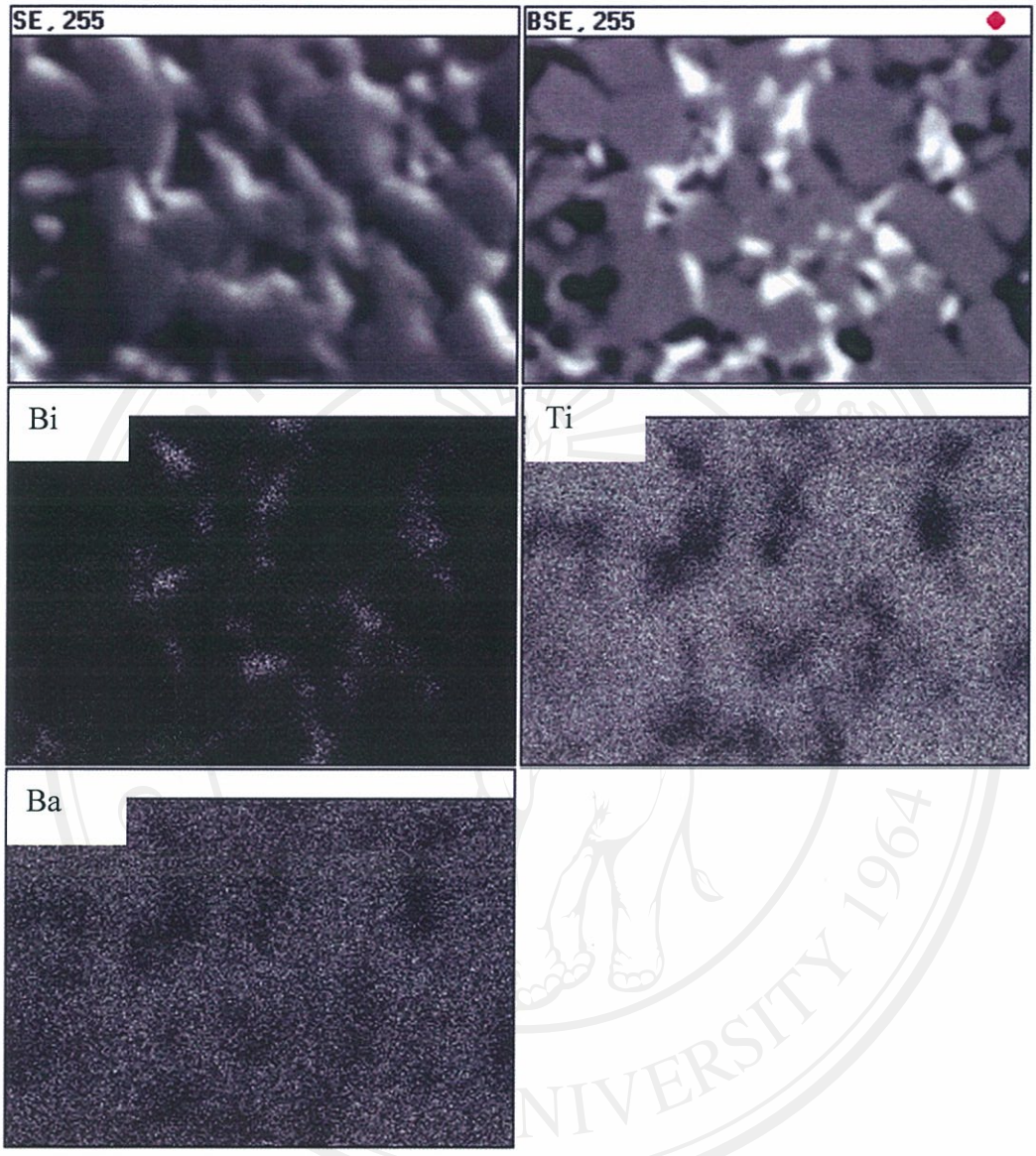

Figure 5.18 Micrographs mapping of Sample B; SE = SEM micrograph, BSE = Backscattering micrograph and the bottom 3 pictures are the X-ray mapping of Bi, Ti and Ba.

The compositional differences within the microstructures were carried out by using back-scattered SEM imaging, along with X-ray mapping and EDX, which was preformed on polished sections of the sintered Sample B, as shown in Figure 5.17-5.18.

The back-scattering images in Figure 5.17 showed coexistence of two phases in bulk ceramic. The white phase is referred to as secondary phase was segregated at grain boundary. The point analysis of EDX showed Bi^{3+} ion was rich in secondary phase along with Ba and Ti ions. Furthermore, the mapping images demonstrated the distribution of Ba, Ti and Bi element as shown in Figure5.18. The mapping images used to be confirmed the EDX data, indicated that Bi cation was segregated at intergranular region as secondary phase. However, we found the Ti diffused out of matrix to form the secondary phase in this system. This result was slightly different that got from the PART II (sintering aids; Bi_2O_3 and Li_2CO_3). Not understood well why the Ti diffused out to grain boundary to form secondary phase. This may be cause by the effect of Pb on the microstructure due to high reactivity than other cation and to promote the substitution at Ba-sites more than segregated at grain boundary. Moreover, this result reflected the substitution of Li^+ and Bi^{3+} at Ti-sites was occurred in this system. To expectation that this effect was reflected by a noticeable increase in tanδ as nominal should be [86, 87]. Due to balance out the charge fluctuation caused by Li^+ will make the interstitial ions unstable, and tanδ is increased abruptly with increasing temperature.

5.10 Dielectric Properties

In general, the coarse grain samples preserve the tetragonal perovskite structure which exhibited high ε_r at sharp phase transition temperature, while the fine grain samples consist of multiphases with the pseudocubic or cubic perovskite structure as a major constituent. Which exhibited a similar flattening to the transition region but with decreased ε_r, which was attributed to the formation of a pseudocubic phase as rhombohedral phase. Due to the substitution of ions with different ionic sizes would distort the lattice structure, corresponding with lower dielectric constants was obtained. When the grain size decreased below 1 μm, the nonlinear ε_r response with temperature was suppressed as shown in Figure 5.19.

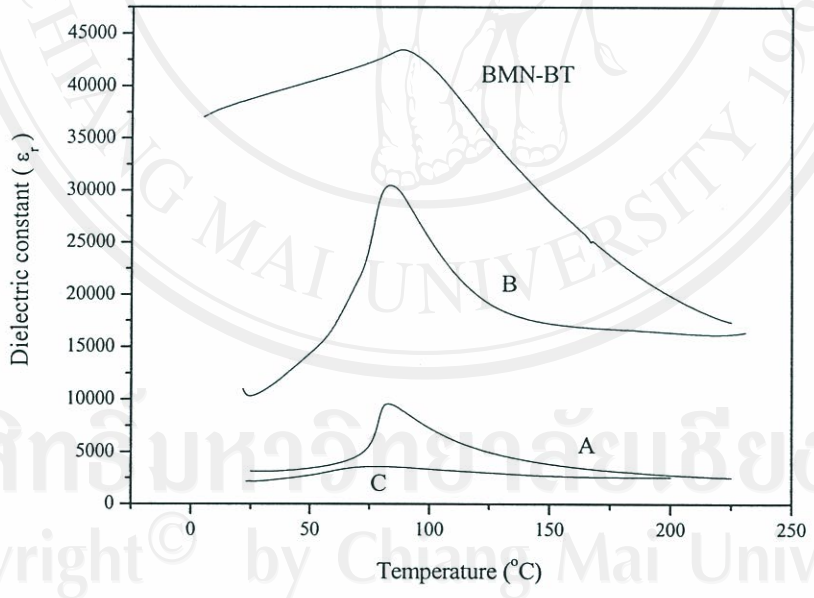

Figure 5.19 Dielectric constant at 1 kHz as a function of temperature for (100-*x*-*y*) $0.02Ba(Mg_{1/3}Nb_{2/3})O_3$-$0.98BaTiO_3$ -xBi_2O_3/Li_2CO_3-$yPbO$ ceramics sintered at 950°C and un-sintering aids.

From the dielectric graph, it was found that the amount of sintering aids had significant decreased the dielectric constant and dielectric curve. The dielectric temperature peak of Sample B is seen much higher than that of Sample A due to the smaller average grain size of Sample B, according to Moulson [8], and the coexistence of tetragonal and cubic phases in this sample. The ε_r value of 30,000 can be reached for grain size 2.85 μm. It should also be noted that this Sample B possesses a relatively high (exceeding 16,500) and invaried ε_r over the temperature range of 100°C to 225°C. This is suitable for MLC capacitors whose applications are in high temperature environment. For samples with large amounts of sintering aids (demonstrated by Sample C), the dielectric temperature peak is suppressed and broadened appreciably due to the presence of the second phase, evidently confirmed by the X-ray diffractogram. Moreover, the chemical gradient was diminished to became chemical homogeneity was found in the fine grain microstructure. This result is reflected by abruptly decreased the dielectric constant at temperature below T_c. Furthermore, it had been found that all sintering aids adding specimens are seen to result in approximately 10°C downshift in the Curie transition to the lower-temperature transition. It is evidenced that the sintering aids could be used as Curie shifter in this system. The maximum dielectric constant ε_{max} and T_c as a function of the concentration *x,y* are presented in Figure 5.20. It should be noted that the ε_r –T characteristics of specimens are intimately related to their microstructure and impurity.

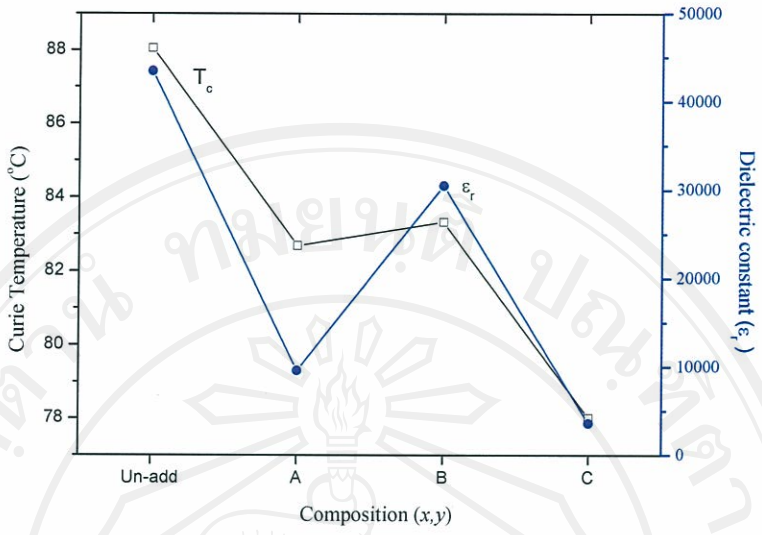

Figure 5.20 Maximum dielectric constant and transition temperature of (100-*x*-*y*) 0.02Ba($Mg_{1/3}Nb_{2/3}$)O_3-0.98$BaTiO_3$-*x*Bi_2O_3/Li_2CO_3-*y*PbO samples sintered at 950°C against composition.

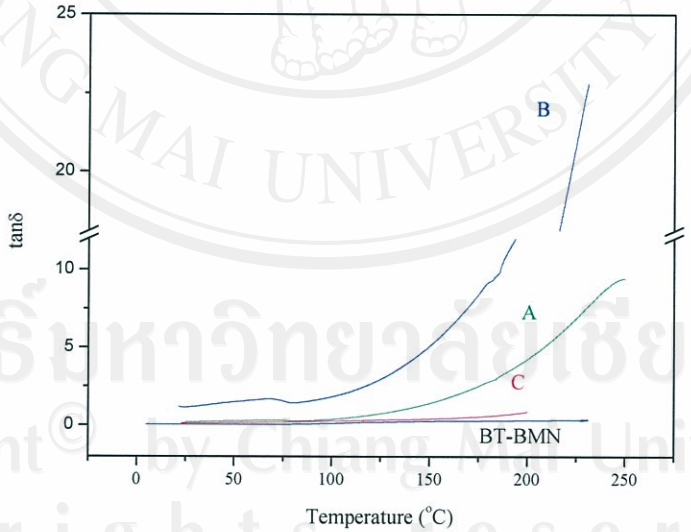

Figure 5.21 Dielectric loss at 1 kHz as a function of temperature for (100-*x*-*y*) 0.02Ba($Mg_{1/3}Nb_{2/3}$)O_3-0.98$BaTiO_3$ -*x*Bi_2O_3/Li_2CO_3-*y*PbO ceramics sintered at 950°C and un-sintering aids.

According to tanδ, Figure 5.21 showed the dependence of the tanδ at 1 kHz. It was observed that Sample C and Un-sintering aids sample, tanδ had a very low value remained constant of about 0.17 and 0.068, respectively. When temperature is higher than 150°C, the curve of tanδ warped upwards markedly within Sample A and B. It may be due to thermal activated space charge conduction which can happen with dielectric and semiconductor at high temperature [45, 66]. Moreover, mobile Li^+ ion and interstitial Li^+ ion in lattice structure will promote the increasing the tanδ as well. The Ti diffused out can confirm by EDX data, indicated Li^+ can replace the Ti-site [77, 86, 87]. More than that this phenomenon was enhanced by chemical defect such as $Bi_{Ba}^{\bullet}$,V_{Ba}'', Li_{Ba}' and $V_O^{\bullet\bullet}$ due to cause by the leakage conductivity. The occurrence of $V_O^{\bullet\bullet}$ in this system due to generate by the formation of hexagonal $BaTiO_3$ was shown in Figure 5.22. This result is given by Lin [84].

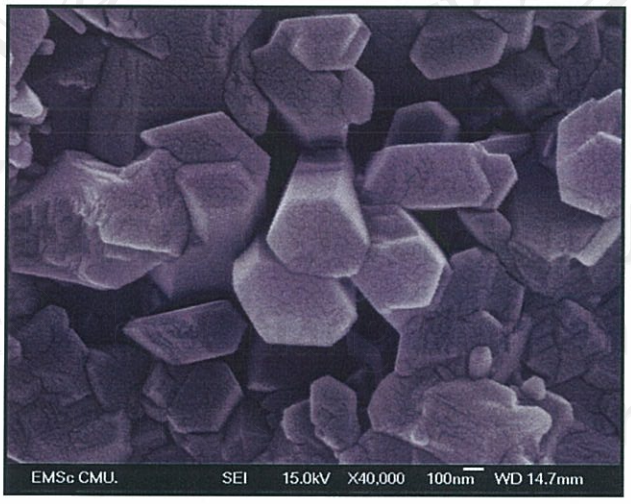

Figure 5.22 SEM micrograph of Hexagonal phase in Sample B sintered at 950°C.

The broadness, δ_γ and diffusivity, γ are estimated by plots of Log [($\varepsilon_{max}/\varepsilon$)-1] versus Log (T-Tm) were plotted as shown in Figure 5.23. The mean value of δ_γ and γ are calculated from equation 4.1. In (100-x-y) 0.02Ba($Mg_{1/3}Nb_{2/3}$)O_3-0.98$BaTiO_3$-xBi_2O_3/Li_2CO_3-yPbO system, the low value of γ and δ significant change in Sample A and B was about 1.22, 7.86 and 1.02, 7.62, respectively. For Sample C exhibited these value was about 1.64, 35.44 which closed to the value of un-sintering aids (BT-BMN) samples but showed poor the dielectric constant compared with un-sintering aids specimen.

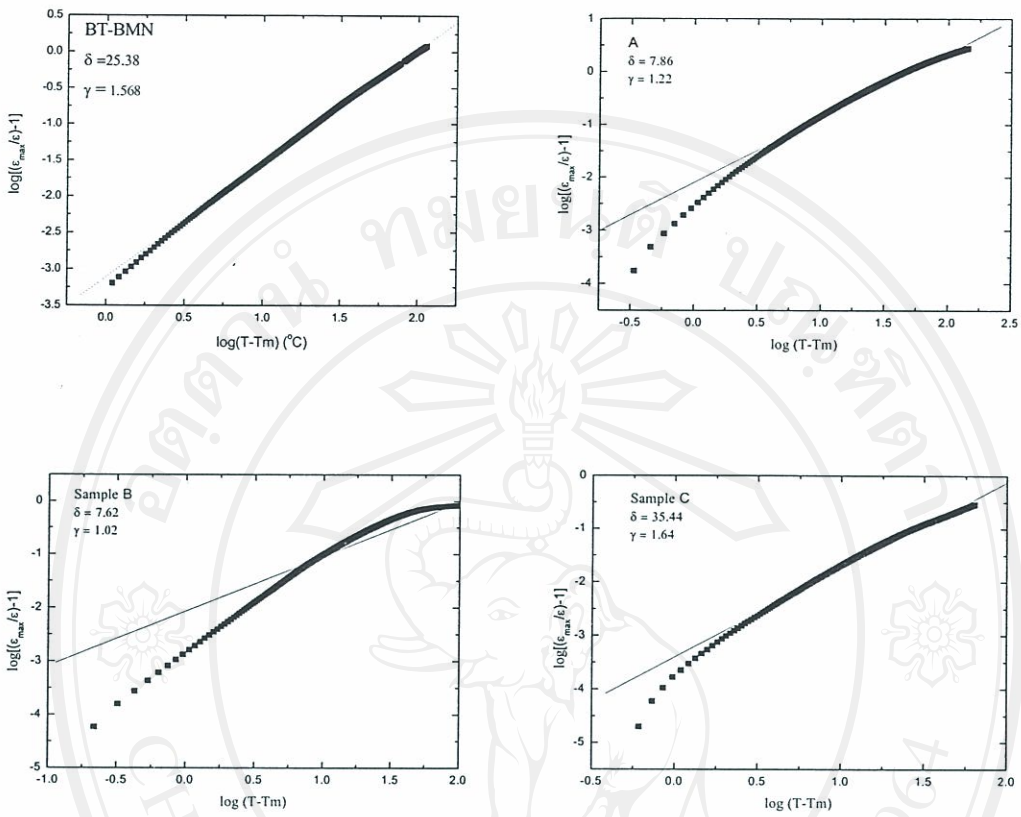

Figure 5.23 Log[($\varepsilon_{max}/\varepsilon$)-1] vs Log(T-Tm) for (100-x-y) 0.02Ba($Mg_{1/3}Nb_{2/3}$)O_3 -0.98$BaTiO_3$-$x$$Bi_2O_3$/$Li_2CO_3$-$y$PbO samples sintered at 950°C and un-sintering aids against composition.